Fuel Processing Technology 250 (2023) 107881

Contents lists available at ScienceDirect

Fuel Processing Technology

journal homepage: www.elsevier.com/locate/fuproc

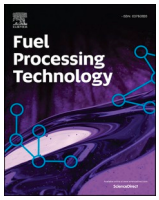

Research article

Characterizing potassium release under turbulent conditions during biomass stream combustion: A comparative analysis of different pretreatments

Cen Sun [a,b,c], Xiaolin Wei [a,c,*]

[a] State Key Laboratory of High-Temperature Gas Kinetics, Institute of Mechanics, Chinese Academy of Sciences, Beijing 100190, China
[b] Department of Energy Power & Mechanical Engineering, North China Electric Power University, Baoding 071003, China
[c] School of Engineering Science, University of Chinese Academy of Sciences, Beijing 100049, China

ARTICLE INFO

Keywords:
Potassium
Biomass
Stream combustion
Tubular flame burner
Ignition
Kinetics

ABSTRACT

The release rate of potassium during biomass combustion significantly influences slagging, fouling, and corrosion in industrial equipment. Given that dispersed biomass stream combustion predominantly occurs under turbulent ambient conditions, we investigate the combustion characteristics and potassium release behavior of rice husk and its derived fuels (water-washed, torrefied, and char) under high-turbulent conditions in a tubular flame burner (TFB). Tunable diode laser absorption spectroscopy (TDLAS) technology, combined with high-speed imaging, was employed to online monitor the release of atomic potassium (K(g)) and the ignition characteristics of biomass stream combustion. The results showed that the rice husk stream followed a joint hetero-homogeneous ignition mechanism, whereas the biochar stream underwent heterogeneous ignition in the TFB. The K(g) peak, occurring ahead of the maximum spontaneous radiation position, was observed at approximately 25 mm from the injectors, with a concentration of 0.067 ppmv during rice husk stream combustion. In contrast, the peak K(g) concentrations for biochar and torrefied rice husk were delayed, reaching 0.026 ppmv and 0.021 ppmv, respectively, compared to the raw biomass samples combusted in the TFB. Distinct differences in activation energy for K(g) release were identified, with pulverized rice husk exhibiting the lowest activation energy (75.53 kJ/mol) and rice husk-char showing the highest (94.20 kJ/mol).

1. Introduction

Increasing carbon emissions and the climate crisis accelerated the transition to biomass utilization, which can be accomplished by retrofitting conventional pulverized coal furnaces. Currently, biomass accounts for over half of all renewable energy sources used worldwide [1], and it is anticipated that biomass usage will play an increasingly important role in the objective of carbon neutrality. Biomass stream combustion is a rapid and adaptable process capable of quickly adjusting thermal power output. Consequently, this process holds the potential to accommodate swift changes in electricity and heat demand caused by intermittent sources like wind, solar, and hydro energy. However, the presence of alkali and alkaline earth metals (AAEMs), notably potassium, in biomass can hinder conversion processes, resulting in downstream corrosion, fouling, and slagging [2,3].

The rate of potassium release is critical due to its significant impact on combustion processes. Diverse combustion approaches can impart distinct effects on the release of potassium during combustion. Consequently, researchers have employed an array of online detection techniques to explore the distinctive characteristics of potassium release in various combustion reactors, including Plane Flame Burners (PFB), Fixed Bed reactors, and Fluidized Bed reactors.

(1) Plane flame burners, such as the McKenna flat flame burner or Hencken burner, are recognized for their high heating rates and compatibility with optical online diagnostics. Several studies have utilized PFB in conjunction with various detection techniques to investigate potassium release during biomass pellet combustion and gasification [4–10]. These investigations have confirmed two distinct gaseous potassium (atomic potassium (K(g)) [6,10] or elemental K [7]) release peaks, attributed to the combustion processes of volatile and char combustion processes [10] and suggested different mechanisms for the alkali metal release process in these two combustion stages [8,9].

* Corresponding author at: State Key Laboratory of High-Temperature Gas Kinetics, Institute of Mechanics, Chinese Academy of Sciences, Beijing 100190, China.
E-mail address: xlwei@imech.ac.cn (X. Wei).

https://doi.org/10.1016/j.fuproc.2023.107881
Received 7 April 2023; Received in revised form 28 May 2023; Accepted 3 June 2023
Available online 22 June 2023

Beyond biomass pellets, He et al. [11] conducted real-time detection for K(g) and atomic sodium (Na(g)) during municipal solid waste combustion in a Hencken burner, founding a singular peak alkali release distribution for plastics combustion process, whereas kitchen waste, papers, and textiles, exhibited a three-stage alkali release pattern. In addition to the biomass pellets combustion or gasification experiments on PFB, Weng et al. [5,12,13] investigated alkali metal (Na*, K*, KCL, and KOH) release during pulverized biomass and bio-char stream jet combustion on a McKenna burner (also known as one of entrained flow reactor), observing Na* and K* emission signals similar to CH* and C2*. **(2)** Fixed beds with optical observation ports, which allow for precise control over the combustion atmosphere, have gained preference among some researchers in detailing combustion atmospheric variations and co-firing effect on the potassium release [14]. Ge et al. [3] investigated alkali-containing species release process in CO_2 gasification of biochar with surface ionization methods, finding distinct differences between wood and straw chars, notably, wood char exhibited stable alkali release throughout most of the process, with a significant increase during the final stage. **(3)** Fluidized bed combustion is a crucial technique for organizing combustion, known for its precise control over the combustion atmosphere and lower operating temperatures. Zhang et al. [15] investigated potassium release from sawdust pyrolysis and gasification within a fluidized bed reactor and found that, between 800 and 900 °C, pyrolysis yielded higher potassium release than CO_2 gasification.

While existing research has significantly advanced our understanding of potassium release during biomass combustion across various combustion methods, fuels, and atmospheres, critical gaps in our comprehension remain, warranting further investigation in this important field. For one hand, pyrolysis and torrefaction, as fundamental steps in the combustion process, are anticipated to be promising biomass fuel pretreatment techniques [16]. Understanding the combined potassium release characteristics and comparing the original and water-washed biomass to examine the release characteristics of potassium in different forms is essential for optimizing biomass-staged combustion processes. This is particularly important as potassium can have adverse effects on biomass-staged combustion industrial technology based on fluidized bed pyrolysis [17]. Despite its significance, previous literature has not thoroughly explored the comparison of a single fuel subjected to different thermochemical pretreatments, such as pyrolysis and torrefaction. Therefore, this study aims to contribute to a deeper understanding of the underlying different pretreatments mechanisms and develop strategies for mitigating the negative impacts of potassium.

On the other hand, the majority of research on alkali metal online detection has been primarily conducted using three types of combustion devices: plane flame burners (PFB) [4–10], fixed bed reactors (FBR) [3,14], circulating fluidized bed (CFB) [15]. The reactors used in these studies (PFB, FBR, and CFB) primarily offer low-turbulence combustion environments with lower flow rates. In industrial equipment, turbulence-chemistry interactions become non-negligible. Since dispersed biomass stream combustion in industrial equipment mainly occurs in turbulent ambient conditions, potassium release kinetic parameters might differ from those derived from the well-reported pellet combustion. Furthermore, from a fundamental perspective, there is a pressing need for mechanistic experimental support to better understand the potassium release process in turbulent biomass stream combustion, as such data is currently limited.

To address these issues, a fully-mixed tubular flame burner was utilized in this work. The tubular flame burner's turbulence intensity and airflow velocity are much greater than PFB or EFR, bringing this ignition technique more representative of pulverized coal/biomass industrial furnaces. In practical powder stream combustion processes, optical opacity within the flame arises from two types of particulate matter: powder particles themselves, ash, and soot generated from the combustion of volatile components. It important for choosing the correct detection method depending on this specific combustion environments. In real-time alkali metal detection within combustion environments, methods like Flame Emission Spectroscopy (FES), Laser Induced Breakdown Spectroscopy (LIBS), and Planar Laser-Induced Fluorescence (PLIF) often struggle with interference from abundant carbon soot and dust. Tunable Diode Laser Absorption Spectroscopy (TDLAS) addresses this challenge with its ability to perform measurements under optically transparent conditions, without interference from either type of particulate matter. Additionally, TDLAS is adaptable to harsh industrial environments, requires no complex calibration, and has lower equipment costs.

This work characterizes the concentration of K(g) release during pulverized biomass combustion in a high-velocity and extremely turbulent environment online using calibration-free TDLAS technology, and captures the stream combustion characteristics of biomass through high-speed photography. A comparative analysis between the K(g) release characteristics of the rice husk (RH) and its derived fuels (water-washed, torrefied, and char) combustion processes were carried out. Temperature-dependent kinetic parameters for K(g) release were then proposed. The experimental data may be quantified to understand the release of potassium and verify numerical simulations, such as CFD simulations of [19,20] potassium-containing fuels combustion, thereby facilitating the investigation of fouling and other related phenomena.

2. Experiments and methods

2.1. Material

The biomass used in this work was rice husk (RH) with a range of 90–120 μm size, and the results of the proximate and ultimate analyses of these biomass materials according to the Chinese national standard (GB/T28731–2012) are shown in Table 1. The RH was subjected to direct pyrolysis at 900 °C for 7 min, followed by a natural cooling process in a nitrogen atmosphere to obtain the RH-char. The torrefied biomass samples were prepared at 250 °C ambient air for half an hour.

Concentrations of total potassium in the RH-char, torrefied-RH, and water-washed RH-char were determined by ICP-OES, as shown in Table 2. The contents of potassium in different forms (water-soluble, exchangeable, organic, and insoluble) were determined using a sequential extraction test [21]. After extraction, the filtrate was measured by inductively coupled plasma-optical emission spectrometry to obtain the amount of potassium in it and, thus, the amount of potassium in different solubilities, as shown in Table 3. Detailed information for the sequential extraction test is shown in the Supplemental Material.

2.2. Combustion system

A schematic diagram of the biomass-central-feeding tubular flame burner (TFB) and its optical diagnostic system is shown in Fig. 1. There are no swirl blades or bluff bodies in the combustion chamber of a tubular flame burner (TFB). The swirling flow produced by the tangential high-velocity jet stabilizes the distinctive tubular flame [22]. The TFB consists of a quartz tube measuring 22 mm in diameter and 50 mm in length, which houses a tubular flame. There are four tangential jets and a central jet nozzle on the bottom of the TFB. The tangential jets are rectangular (6.3 mm × 1.5 mm) and inject a mixture of oxygen and nitrogen, while the other jets inject a mixture of methane (CH_4) and nitrogen. The high-speed tangential spinning facilitates the quick mixing of the gases, producing a methane-air tubular flame. Both tangential and central jets located at the bottom of the tubular flame burner center can be employed for the injection of pulverized biomass into the burner. When utilizing the central feeding method, the finely ground biomass is capable of remaining in the high-temperature zone at the center of the burner for a prolonged period, thus promoting its combustion.

The biomass stream, produced through the operation of a helical vibrating micro feeder at a constant flow rate of 0.325 g/min, is subsequently introduced into the TFB chamber through the central jet

Table 1
Proximate and ultimate analysis for biomass.

Sample	Proximate analysis w_{ad}/%				Ultimate analysis w_{ad}/%				
	M	A	V	FC	C	H	O	N	S
Rice husk	7.71	10.23	68.93	13.13	37.14	5.18	39.41	0.30	0.03

Note: ad = air dry basis.

Table 2
Concentrations of potassium in the sample after different pretreatments.

Biomass	Total potassium (wt%)
RH-char	0.5573
Torrefied-RH	0.5697
Water-washed RH-char	0.1799

Table 3
The amount of potassium in different solubilities in the Rice husk (RH).

Forms of potassium	Percentage by weight (wt%)
Total	0.198
Water-soluble	0.159
Exchangeable	0.032
Acid-soluble	0.005
Insoluble	0.002

nozzle (4 mm diameter) located at the bottom of the burner. The gas compositions and flow rates at each site are detailed in Table 4. Among these, the center jet flow rate is only 5% of the tangential input gas flow rate, ensuring that the center jet's influence on the tubular flame is insignificant. The temperature distribution along the burner's centerline was monitored with a radiation loss compensated type B thermocouple of 200 μm, as shown in Fig. 2.

Computational fluid dynamics simulations (CFD) were employed to elucidate the particle temperature histories within the TFB. Both the Reynolds Stress Turbulence Model and the Discrete Phase Model (DPM) were activated in the CFD simulation. Fig. 3 presents the particle temperature histories as a function of height following the injection of particles into the TFB. This detailed analysis allows for a comprehensive understanding of the temperature dynamics within the system. More detailed results for CFD simulation are available in the Supplemental Material.

2.3. Potassium detection methods

It important for choosing the correct detection method depending on the specific combustion environments. LIBS provides swift, multi-element detection, effectively identifying atomic [8,9,23] and elemental forms of potassium [7,24], it may have limitations in identifying specific compounds like KOH. Its accuracy can be influenced by laser power variations, spectral interference, and the presence of soot and ash. PLIF [7] offers remarkable sensitivity and outstanding temporal and spatial resolution in detecting atomic potassium, it may not directly detect specific compounds like KOH. It may be subject to quenching effects and interference from soot and ash, necessitating calibration under certain circumstances. FES typically measures atomic potassium [11]. It is simple to implement with modest equipment requirements but can be compromised by soot/ash interference and low analyte concentrations. UV spectroscopy mainly detects certain potassium ions (KOH (g), KCL(g)) [25–27]. It offers excellent sensitivity and specificity but may be limited by potential overlap of emission lines and the requirement for a clean optical path. TDLAS excels in providing highly sensitive and accurate measurements under optically transparent conditions, remaining unaffected by particulate matter. TDLAS eliminates the need

Table 4
Gas flow rate for the tubular flame burner.

Fuel-side tangential injectors (L/min)		Oxidizer-side tangential injectors (L/min)		Central jet for biomass (L/min)
CH_4	N_2	Air	O_2	Air
0.9	12	8	6	1.5

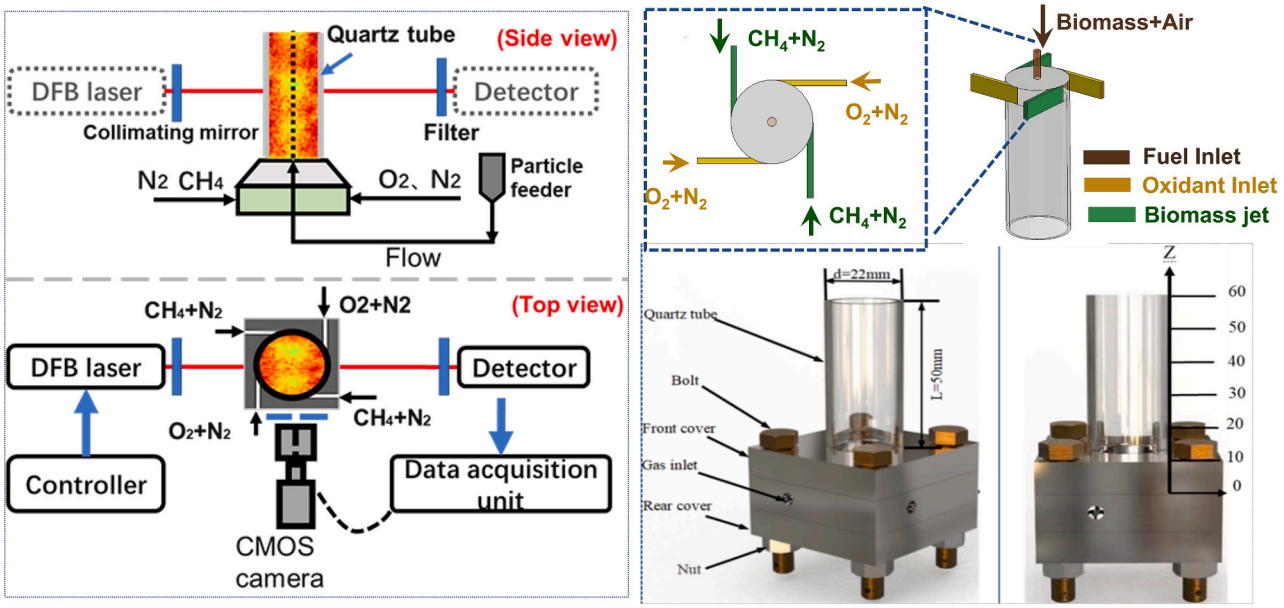

Fig. 1. Schematic diagram of the central-feeding tubular flame burner and its optical diagnosis system.

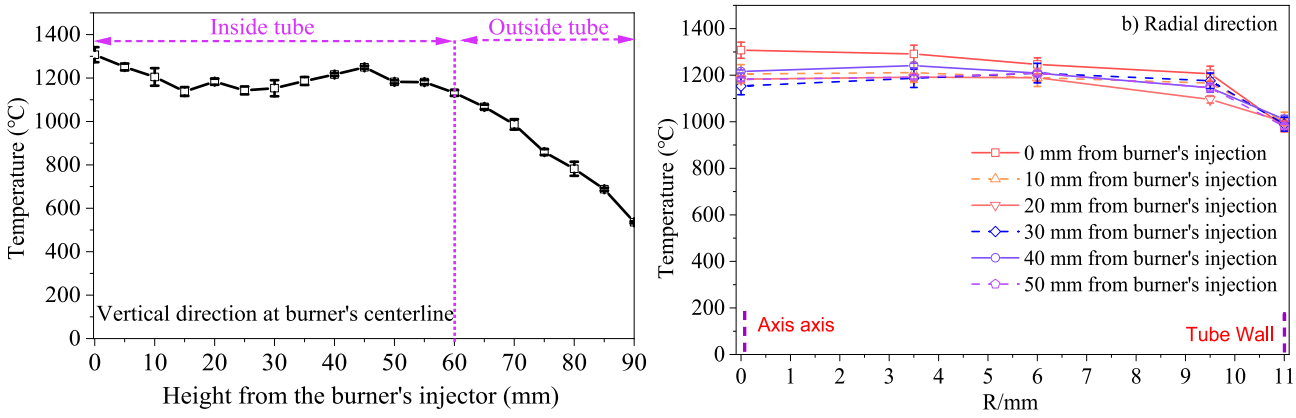

Fig. 2. The tubular burner's temperature distributions in the chamber of the TFB, a) Vertical direction at the burner's centerline, b) Radial direction.

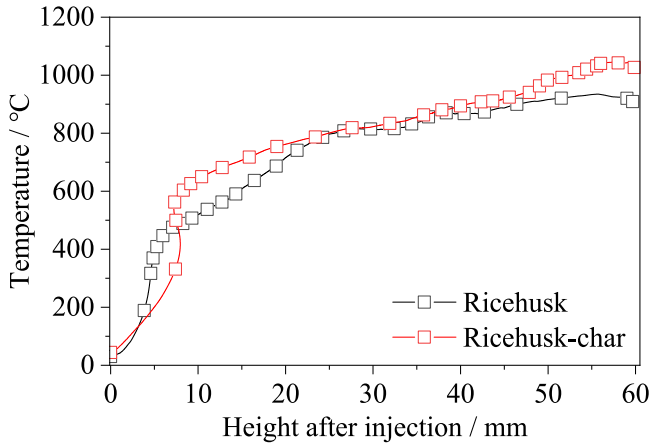

Fig. 3. Particle temperature histories and residence time as a function of height after injection.

for complex calibration and is well-suited for harsh industrial environments [28]. However, its performance may be limited in applications involving optically opaque conditions and specifically effective in measuring atomic alkali metals. TDLAS has been employed to measure atomic potassium (K(g)) in various environments and expanded the technique's application to a pilot-scale biomass gasification reactor, thus investigating the reliability of TDLAS for K(g) measurement [4,28–33]. Therefore, this work utilizes TDLAS to detect K(g) release during the combustion process. The distribution of temperature and oxygen can be used to infer the presence of other potassium compounds through the gas-phase reaction mechanism of potassium.

The version of TDLAS used in this work is the direct detection of absorption (DAS). For DAS-TDLAS, concentration or signal processing hardware calibration is not required [34]. The light source of the TDLAS system employed in this work was a distributed feedback laser diode (Nanoplus-TO56–770 nm) with a scanning frequency of 30 Hz. Light intensity changes were recorded using a photodetector (ThorLabs-DTE100A/M). The Voigt line profile was used to fit the absorbance curve. The optical path length was determined by the inner diameter of the quartz (22 mm), which confined the tubular flame. Fig. 4 shows the typical spectroscopic scanning of the potassium D_1 line (scattered points) and the Voigt profile (solid line). At an optical path length of 2.2 cm, the TDLAS system employed in this work has a lower detection limit of 7 ppbv and an upper detection limit of 1050 ppbv for K(g). At high concentrations, the goodness of fit of the absorption line exceeds 0.99. At lower concentrations, the absorption signal was easily drowned in the

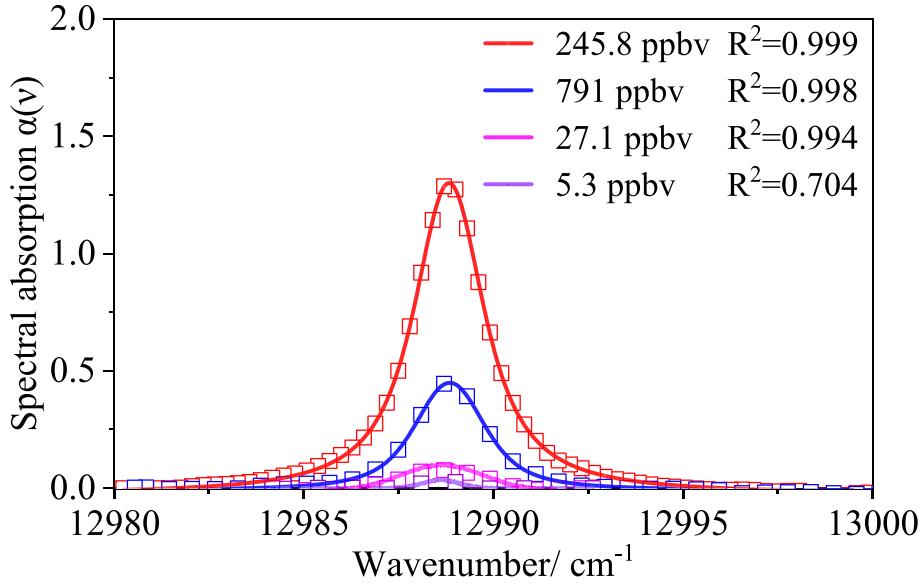

Fig. 4. Typical spectroscopic scanning of the potassium D_1 line ($4^2S_{1/2} \rightarrow 4^2P_{1/2}$). The absorbance spectra obtained from the measurements are represented as scattered data points, while the solid lines depict the Voigt curve fits applied to these data points.

baseline noise, reducing the goodness of fit of the absorption line to 0.7. The target gas's concentration C can be expressed as:

$$n = \frac{c}{h\nu_0 B_{12} L}\int_{-\infty}^{\infty} \alpha(\nu)\mathrm{d}\nu \quad (1)$$

$$C = \frac{nM_r}{N_A} \quad (2)$$

where c represents the speed of light, h denotes Planck's constant, ν_0 is the central frequency. Furthermore, B_{12} stands for the Einstein absorption coefficient, L signifies the optical path and $\alpha(\nu)$ corresponds to the spectral absorption coefficient. Additionally, $n$is the molecular number density, Mr. represents the relative molecular mass, and N_A is the Avogadro constant. A detailed theory for laser-based K(g) detection is described in the Supplemental Material.

A CMOS camera with a 105 mm macro lens was used to directly detect the visible light intensity of the biomass combustion process in the TFB chamber with a maximum picture size of 5472 × 3648 pixels.

3. Results and discussion

The combustion process is strongly coupled to the potassium release process; thus, the stream combustion process of biomass was discussed first, followed by the potassium release characteristics.

3.1. Combustion characteristics of biomass stream combustion

Visible light has proven to be a good indicator of ignition, with ignition occurring at 15% of the normalized max intensity [5,35–37]. Hence, snapshots of pulverized biomass and its biochar combustion process within the TFB were captured to determine their ignition properties.

To quantitatively detail the ignition position of the pulverized biomass, after subtracting background signals, the two-dimensional snapshots were converted to grayscale and then horizontally projected, i.e., the grayscale values of the pixels with the same distance from the injectors of the TFB were accumulated to determine the grayscale distribution values along the z-axis of the TFB. In addition, the maximum gray value was set for normalization to eliminate the effect of the fluctuating powder feeding rate.

Fig. 5 portrays a detailed snapshot of the combustion progress and axial distribution of visible light intensity during the pulverized rice husk (RH) and water-washed RH stream combustion in the TFB. The snapshots were captured with a 1/40 s shutter speed and an ISO of 500 to capture the combustion process effectively. Upon feeding the pulverized RH into the TFB, it was immediately accelerated by the spinning tangential airflow loop and eventually obtained tangential velocity. With the acquisition of tangential velocity, the pulverized RH was propelled upward by centrifugal forces as they reached the inner wall of the quartz tube. As the pulverized samples reached a certain distance from the injectors of the TFB, the visible light intensity reached its maximum value. The ignition points of pulverized RH occurred approximately 10.5 mm from the TFB injectors, and the maximum visible light intensity occurred at approximately 34 mm for the pulverized RH combustion process. Compared to the raw sample's combustion, the water-washed samples exhibited an increased ignition delay, as evidenced by the ignition position of approximately 12.0 mm from the TFB injectors. This ignition delay may be due to the removal of water-soluble K, Na, Cl, and S elements from the biomass during the washing process. The removal of these species from the biomass could cause a significant decrease in their catalytic effect on the combustion process [38], resulting in a delay in the ignition of the biomass powder after washing. Deng et al. [39] also found that volatiles was released at higher temperatures during water-washed biomass combustion compared to the original biomass combustion in a thermogravimetric experiment.

Fig. 6 demonstrates the combustion process of pulverized rice husk char (RH-char) and torrefied RH within the TFB. Upon ignition, the visible light intensity peaked and then gradually diminished. The RH-char ignited about 12 mm from the TFB injector, presenting a slight delay compared to the original biomass. This delay in ignition might be attributed to the pyrolysis process, which releases most of the volatile components as gases, primarily leaving behind carbonaceous material. This carbonaceous material, due to its higher ignition temperature, could potentially account for the delayed ignition. In contrast, torrefied RH was found to ignite at a distance of less than 10 mm from the TFB injector. This signifies improved ignitability, might attributed to the reduced moisture content and increased energy density acquired through torrefaction. The precise ignition point was not determined due

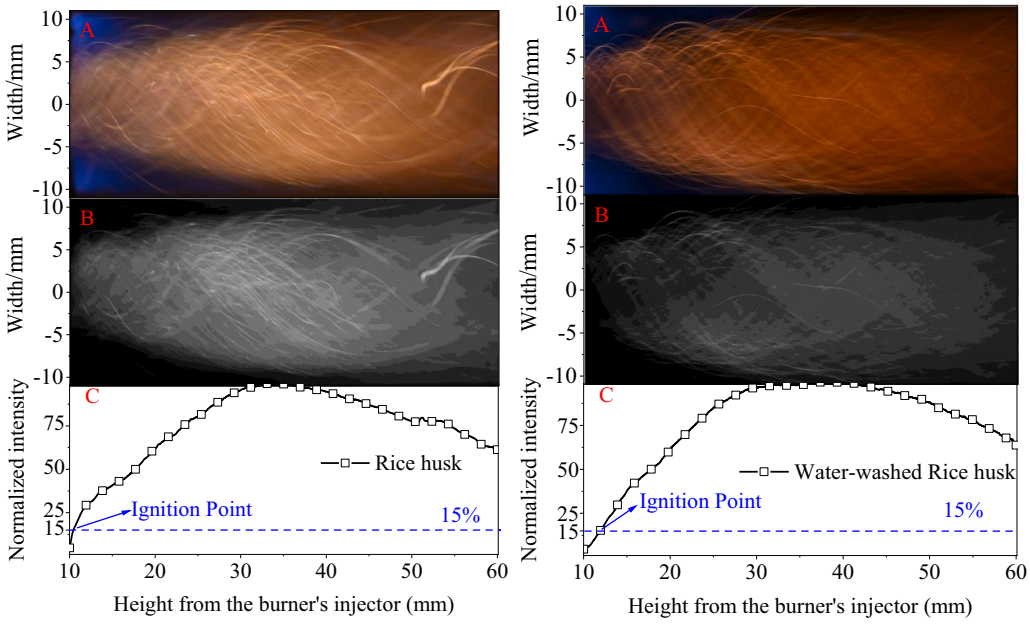

Fig. 5. Snapshot of the pulverized RH and water-washed RH combustion process in the TFB. Captured with a 1/40 s shutter speed and an ISO of 500. A, original snapshots; B, grayscale snapshots after background subtraction; C, the z-axis distribution of visible light intensity.

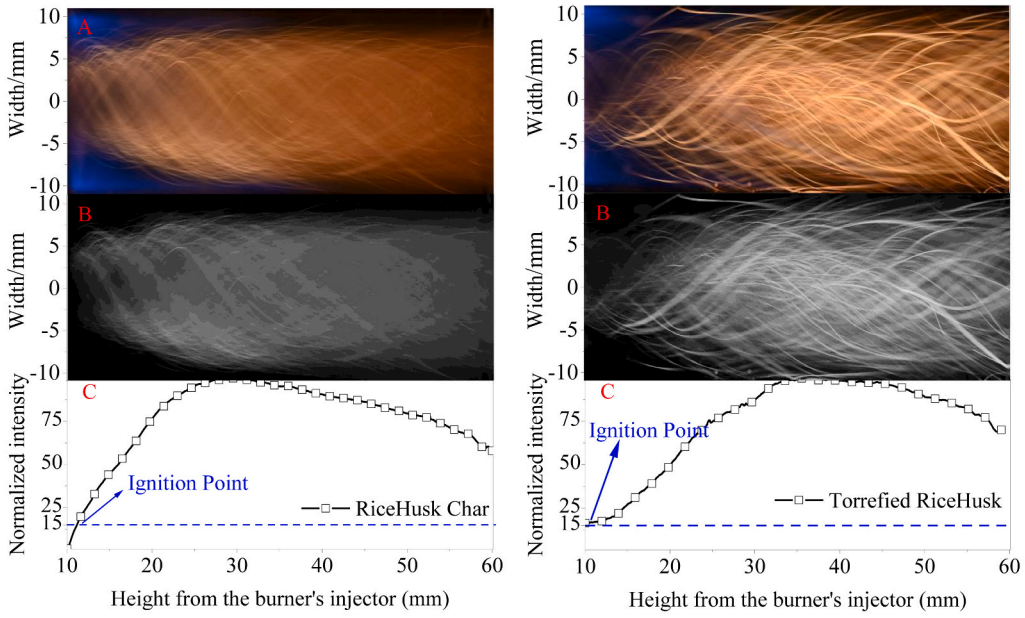

Fig. 6. Snapshot of pulverized biochar and Torrefied RH combustion in the TFB. Captured with a 1/40 s shutter speed and an ISO of 500. A, original snapshots; B, grayscale snapshots after background subtraction; C, the z-axis distribution of visible light intensity.

to partial visual obstruction by the burner's front cover. Our results underscored the critical role of thermal treatment methods in modulating ignition behavior and further exploration is encouraged to optimize these processes for enhanced combustion performance. A comparative analysis of the combustion process images for pulverized RH-char and raw pulverized RH samples within the TFB uncovers a notable difference in the trajectories of the RH-char. The path followed by the RH-char (represented by the spiral line of high intensity in the images) exhibited greater regularity and uniformity in brightness. This contrast can be attributed to the anisotropic release of volatiles during the combustion of raw pulverized RH samples, which subsequently altered the direction of particle movement and diminished the regularity of the upward spiral trajectory. Llamas [40] observed a similar phenomenon: approximately 37% of biomass fine particles in a high-velocity jet experienced sudden acceleration during the rapid devolatilization process. This occurrence, referred to as the "rocket" process, further substantiates the impact of the volatile release on particle movement during combustion.

To elucidate the ignition process of the pulverized RH stream within the TFB, high-speed images were captured for analysis. Fig. 7 illustrates that upon introducing pulverized RH and RH-char into the TFB chamber, the fine biomass particles quickly ignited on the surface without a surrounding envelope of volatile flame. As the particles spiraled forward, a flame cloud enveloped the brightly burning particles, which resulted from the continuous heating of the RH powder in the chamber, leading to volatile ignition and the generation of an envelope flame. The ignition mechanism of pulverized RH in the TFB exhibited hetero-homogeneous characteristics, which contrasts with the typical homogeneous ignition mechanism observed in pulverized biomass within visual drop-tube furnace [41] or planar flame burners [5,38,42]. The high-speed and high-turbulence environment in the TFB chamber potentially facilitated heat and mass transfer around the particles, giving rise to non-

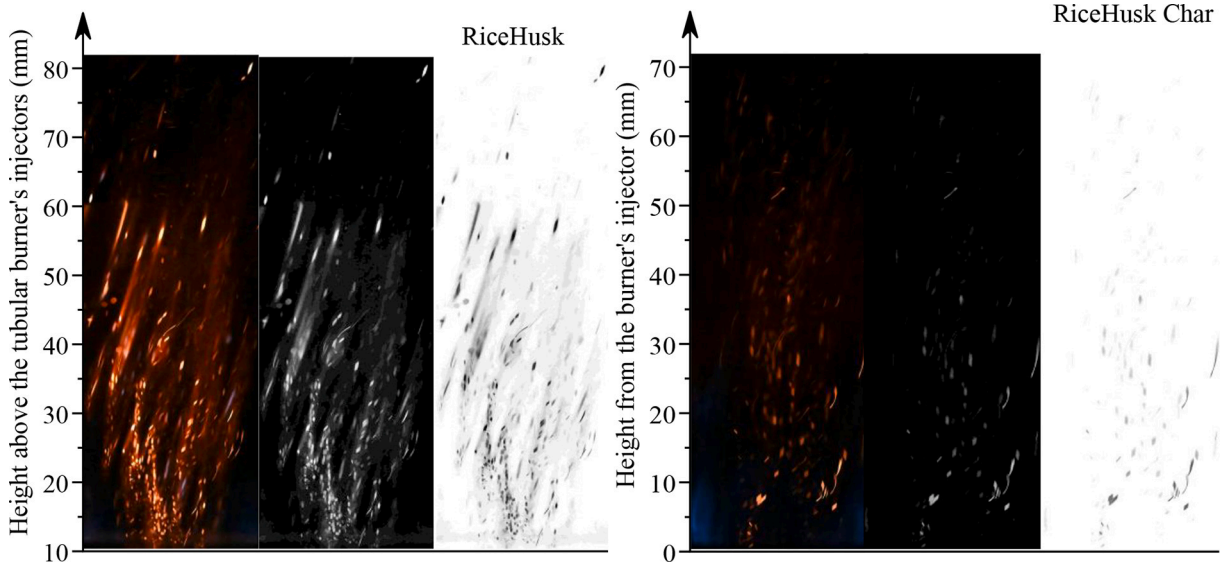

Fig. 7. High-speed combustion images of pulverized RH and RH-char. The exposure time was 1/8000 s.

homogeneous combustion reactions on the particles' surfaces.

As the pulverized RH-char powder ascended along a spiral trajectory within the tube, the intensely luminous particles progressively diminished in brightness and ultimately extinguished. This occurrence unfolded in the absence of an envelope flame, which lends further support to the notion that heterogeneous ignition characterizes the RH-char combustion process.

3.2. Potassium release characteristics

The pulsation of the spiral vibrating micro sample powder feeding speed was considered to ensure accurate measurements. At each measuring point, continuous sampling for five seconds was employed to eliminate irregularities caused by the fluctuation in the powder feeding rate, which is a common problem encountered during pulverized biomass combustion [59,60]. Consequently, gross errors were subsequently eliminated, allowing for the calculation of the mean K(g) concentration. This is particularly important when determining the real-time signal of the K(g), as shown in Fig. 8.

Fig. 9 depicts the K(g) distribution in the TFB for raw RH and the water-washed RH stream combustion process. During the raw pulverized RH powder stream combustion, two K(g) release peaks were observed along the z-axis of the TFB. The first K(g) concentration peak, situated 25 mm from the injections, measured 0.071 ppmv, while the second peak, 0.036 ppmv, appeared approximately 60 mm after the injection. Though direct data regarding potassium release in highly turbulent environments are scarce, similar experimental results can be referenced. Zhu et al. [23] observed a bimodal release pattern for sodium and potassium during the combustion of dispersed Zhundong coal streams in a downstream laminar flow reactor. In conjunction with the results shown in Fig. 7, it can be seen that the K(g) release peak rate corresponded to the jointed hetero-homogeneous combustion stage of pulverized biomass, both of which preceded the maximum spontaneous radiation light intensity position.

For water-washed pulverized RH, only a single wide K(g) concentration release peak was observed, with the maximum concentration of K(g) appearing approximately 40 mm from the injectors, measuring 0.018 ppmv. The water-washing process, which removes water-soluble inorganic potassium from the biomass [23], effectively eliminates 80.3% of potassium in RH, leading to a significantly decreased K(g) concentration during the combustion process of the water-washed sample.

Considering the water-soluble potassium release mechanism, a portion of water-soluble potassium is directly released through vaporization during the drying and devolatilization stage, while the remaining portion is converted into char-bonded potassium, as demonstrated in reactions R1 and R2 [47–51]. This observation suggests that the release of organic and exchangeable potassium primarily occurs within the 40–60 mm range from the injection point. At the same time, the release process of char-bonded potassium might take place at a longer distance (60–90 mm) from the burner's injectors.

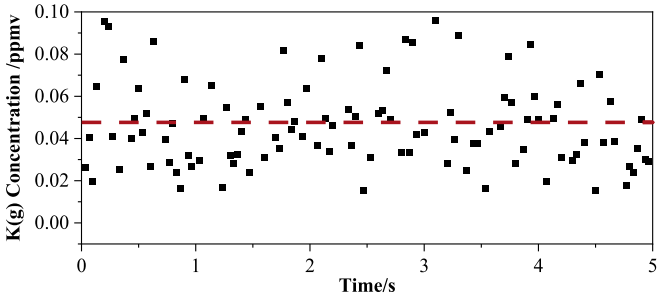

Fig. 8. K(g) concentration's real-time TDLAS signal.

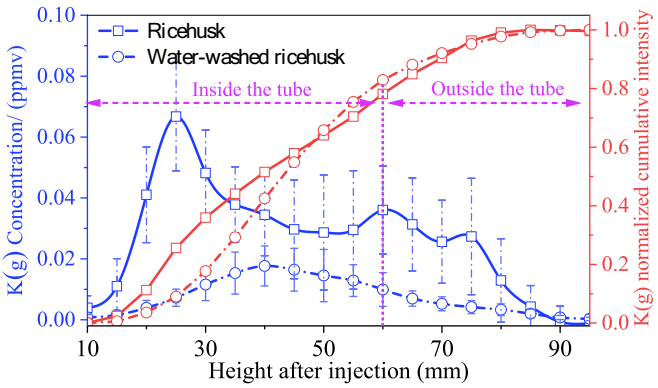

Fig. 9. K(g) concentration during RH and water-washed RH stream combustion process in the TFB.

$$KCL(s) \rightarrow KCL(g) \quad \text{R1}$$

$$R - COOK \rightarrow Char - K \quad \text{R2}$$

As shown in Fig. 10, the K(g) concentration for the pulverized RH-char and torrefied-RH combustion process in the TFB were nearly identical. This finding aligns with the inductively coupled plasma-optical emission spectrometry (ICP-OES) test results, which showed that the total potassium content in RH-char and torrefied-RH was also the same, as presented in Table 2. For the RH-char and torrefied-RH combustion processes, the K(g) concentration increased at a slower rate along the z-axis in the range of 10–50 mm, and the maximum peak of K(g) appeared ~50 mm from the injectors of the TFB with concentrations of 0.026 ppmv and 0.021 ppmv, respectively. The peak values of K(g) released by the torrefied biomass and RH-char were delayed compared with those of the raw biomass samples combusted in the TFB. Between 10 and 20 mm from the TFB injectors, the K(g) concentration in water-washed RH-char combustion increased steadily and remained almost constant from 20 to 45 mm. The K(g) concentration released within the water-washed RH-Char stream combustion process was significantly lower than that of the original RH-Char stream, indicating that the potassium released from the RH-char was predominantly water-soluble. Weng et al. [13] carried out a quantitative observation of the potassium release process during the biochar stream combustion. They found that the potassium release followed a single-peak distribution, where a higher initial potassium content in the biochar led to an increased release rate. (See Fig. 11.)

A widely accepted explanation posits that during the torrefaction process, some potassium species undergo conversion from a water-

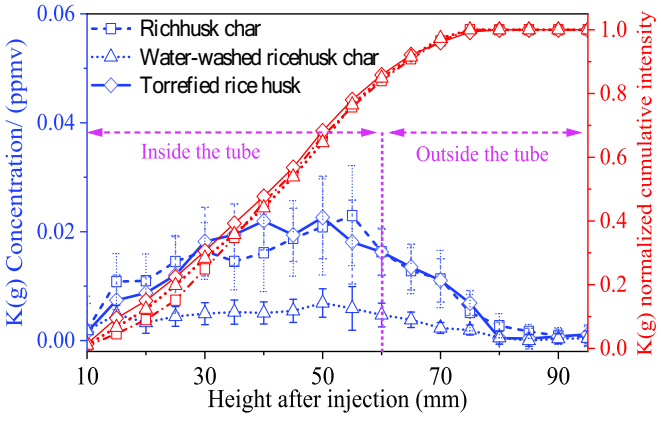

Fig. 10. K(g) concentration during RH-char, water-washed-RH-char, and torrefied-RH stream combustion processes in the TFB.

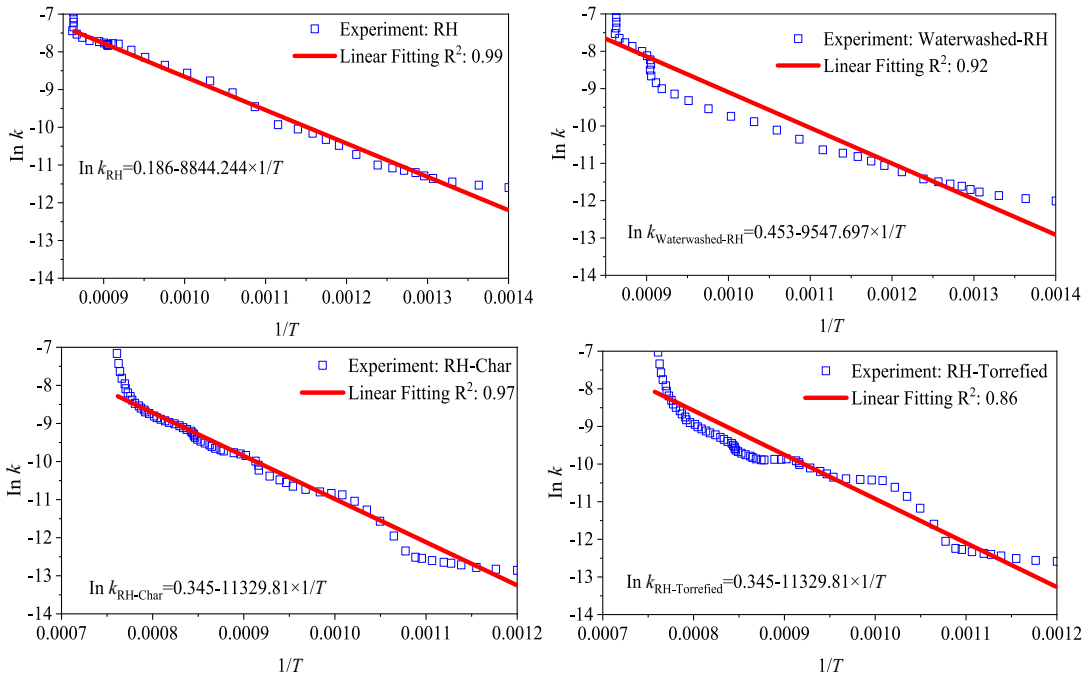

Fig. 11. K(g) release rate constants for the rate-determining steps.

soluble state to an ion-exchanged or organic state [52], as outlined in reactions R_3 and R_4 [53–57]. Ion-exchanged or organic potassium is more prone to retention in the char at high temperatures, making it challenging to release.

$$KCL(s) + Organic(s) \rightarrow Organic - K(s) + HCL/CH_3CL/tar - CL \quad R3$$

$$R - COOH + KCL \rightarrow R - COOK + HCL \quad R4$$

3.3. Kinetic analysis of K(g) release

Based on online detection data, many studies have attempted to describe the release behavior of pelleted biomass [24,46,57]. Van Eyk et al. [47] estimated the sodium release rate constant (k) by examining the relationship between particle surface temperature and the sodium release process, as shown in eqs. (3–4).

$$\frac{dw}{dt} = -k \cdot w \quad (3)$$

$$k = A \times exp\left(-\frac{E}{RT}\right) \quad (4)$$

In the given equation, R denotes the universal gas constant, E represents the activation energy, and T corresponds to the particle's temperature. Additionally, A stands for the frequency factor, and w is the cumulative fraction of released K(g) [24]. Fatehi et al. [8,9] suggested that the potassium release rate for biomass pellets combustion in a plat flame burner follows a first-order Arrhenius equation during the char and ash reaction stages, with activation energies ranging between 218 and 248 kJ/mol and 168–198 kJ/mol, respectively. In a similar setup, for pinewood char combustion in a plat flame burner, Zhang et al. **[59]** obtained kinetic parameters for K release (89.9 kJ/mol for the activation energy and 12.5 1/s for the pre-exponential factor). The reported kinetic parameters of potassium release directly from a biomass stream's combustion have not been well detailed, which might differ from those of the reported pellet combustion. Further kinetic data is needed for potassium release characteristics in high-velocity and turbulent stream combustion, which is also desired for CFD simulation of the potassium-containing fuels combustion process [20,21].

The normalized K(g) release rate was determined by the cumulative fraction of released K(g) (w) through Eq. (3), as shown in Fig. 9 and Fig. 10. As observed from the combustion images in Section 3.1, the trajectory of the particles in the TFB exhibited a three-dimensional spiral, making it difficult to experimentally measure individual particle surface temperatures at various moments (locations). Consequently, we conducted a computational fluid dynamics simulation to speculate the temperature profile of the particles, as demonstrated in Fig. 3. The activation energy and frequency factor were then calculated by the intercept and slope in the Arrhenius plot (In k versus $-1/T$), respectively, as shown in Table 5.

As seen in Table 5, the activation energy for K(g) release of the water-washed RH combustion process was elevated compared to the raw RH. This could primarily be attributed to the fact that water-soluble inorganic potassium is released more readily than organic potassium, and the water-washing process removes this water-soluble inorganic potassium from the biomass. During torrefaction, the inorganic potassium is converted to organic potassium, which may result in the kinetic parameters of K(g) release from torrefied RH being similar to those for water-washed RH. The activation energy of the K(g) release process in the RH-char combustion process is the highest, which may be due to two reasons: firstly, after volatile analysis, only char-bonded potassium is retained, which is more thermally stable than inorganic and organic potassium; secondly, the char combustion process lacks the physical carrying effect of Stephen's flow on the potassium release.

The reported activation energy of alkali metals (Na, K) release for biomass pellets static combustion process, as summarized in Table 6,

Table 5
Kinetic parameters for K(g) release of the biomass combustion process in the TFB.

Parameters	Pulverized RH	Water-washed RH	Torrefied-RH	RH-char
The activation energy (kj/mol)	73.53	79.38	97.46	94.20
Frequency factor (s^{-1})	1.20	1.57	2.22	1.41

ranges from 80 to 266 kJ/mol. In comparison, the activation energy for the stream combustion process of pulverized RH in the TFB was lower. The reduced diameter of the pulverized biomass could provide a larger reaction surface area and a higher heating rate. Simultaneously, the high velocity and high turbulence ambition in the TFB also enhanced the heat and mass transfer on the particle surface. These factors might constitute the major explanation for activation energy reduction.

4. Discussion

Potassium is known to be released in different forms such as KCL(g), KOH(g), and K(g) during the combustion process. Under conditions of high-speed and high-dust stream flames, it remains challenging to accurately measure gaseous KOH(g) and KCL(g). Given technical limitations, our study only focused on the measurement of potassium atoms under high-dust, high-turbulence stream combustion conditions that have not been extensively studied before.

Computational methods, like thermodynamic calculations or detailed reaction mechanisms, play a crucial role in this research. Combining this experimental concentration data of K(g) with thermodynamic calculations [8,47] and detailed reaction mechanisms could indeed provide a more comprehensive understanding of total gaseous potassium release during biomass combustion, even if we cannot directly measure various potassium forms. Future research should incorporate theoretical methodologies (thermodynamic calculations or detailed reaction mechanisms) in conjunction with our experimental investigations to get a more comprehensive understanding of the potassium release process during biomass combustion.

Indeed, the development of advanced methodologies for precise measurements of KOH(g) and KCL(g) in high-dust environments is imperative. Moving forward, thorough exploration of potassium release during high-turbulence stream combustion, especially deriving kinetic parameters from gaseous KOH(g) and KCL(g) data, is of paramount importance. These pursuits will furnish a more detailed understanding of the potassium release process, augmenting our grasp of biomass combustion.

This work offers initial insights into the intricate process of potassium release in the context of high-turbulent and high-dust stream combustion. It is intended to stimulate further inquiries in this domain, encouraging scholars to probe deeper into this compelling and pivotal area of research.

5. Conclusion

Given that dispersed biomass stream combustion, exhibits rapid adaptability to fluctuations in renewable energy demand, predominantly occurs under turbulent ambient conditions. In this work, we have made a preliminary effort to examine the combustion characteristics and potassium release behavior of rice husk (RH) and its derived fuels (water-washed, torrefied, and char) under high-turbulent conditions in a tubular flame burner (TFB). Based on the experimental findings, the following conclusions can be drawn:

(1) Under the investigated conditions, the ignition delay of pulverized biomass in a TFB was notably shorter than that reported in a planar flame burner. High-speed camera images revealed the hetero-homogeneous ignition mechanism for raw rice husk, characterized by an enveloping volatile flame surrounding the burning particle. Conversely, rice husk char experienced a purely heterogeneous ignition process.
(2) The K(g) peak position was ahead of the maximum spontaneous radiation position. The maximum K(g) concentration for rice husk stream combustion appeared approximately 25 mm from the injectors (0.067 ppmv). The peak value of K(g) released by the torrefied biomass and biochar was delayed compared with that of the raw biomass samples combusted in the TFB, with concentrations of 0.026 ppmv and 0.021 ppmv, respectively. The maximum K(g) concentration for the water-washed RH, with 0.018 ppm, was 40 mm downstream of the injection point.
(3) The activation energy for K(g) release varied among the different biomass samples. The pulverized rice husk stream combustion exhibited the lowest activation energy (73.53 kJ/mol). Water-washed rice husk demonstrated a higher activation energy (79.38 kJ/mol) compared to raw rice husk, and its kinetic parameters were similar to those of torrefied rice husk (97.46 kJ/mol). The highest activation energy was observed during the combustion process of rice husk-char (94.20 kJ/mol).

Table 6
Summary of kinetic parameters of the heterogeneous release of solid alkali metals.

Fuel shape	Reactor	Species	Frequency factor (s^{-1})	Activation energy (kJ/mol)	Ref.
Pulverized biomass (64–75 μm)	Laminar flame burner	Atomic Sodium	$10^{1.16}$	87.2	[23]
Single Poplar pellet (4 mm)	Laminar flame burner	Total potassium	$A_1 = 4.64$ $A_2 = 20.5$	$E_1 = 84.6$ $E_2 = 55.4$	[7]
Single Corn straw pellet (4 mm)	Laminar flame burner	Total potassium	$A_1 = 2.24$ $A_2 = 15.3$	$E_1 = 64.8$ $E_2 = 62.8$	[7]
Single Swedish wood pellet (diameter of 8 mm and height of 4 mm)	Laminar flame burner	Total potassium mass and sodium mass	$A_K = 5.3 \times 10^{10}$ $A_{Na} = 3 \times 10^{12}$	$E_K = 185$ $E_{Na} = 223$	[8]
Single pinewood pellet (3–4 mm)	Laminar flame burner	Total potassium mass	12.51	89.9	[59]

These combustion characteristics and potassium release behavior of rice husk and its derived fuels under high-turbulent conditions might provide valuable information for future studies aimed at numerical simulations and mitigating slagging, fouling, and corrosion issues in biomass combustion systems and can contribute to the development of more efficient and environmentally friendly biomass utilization technologies.

CRediT authorship contribution statement

Cen Sun: Writing – original draft, Conceptualization, Methodology, Software, Investigation, Formal analysis, Writing – review & editing. **Xiaolin Wei:** Conceptualization, Funding acquisition.

Declaration of Competing Interest

The authors declare that they have no conflict of interest.

Data availability

Data will be made available on request.

Acknowledgment

The author acknowledges the support of the National Science Foundation of China for this work (No. 51736010). The author thanks Professor Fei Li and Teng Li for discussing TDLAS.

Appendix A. Supplementary data

Supplementary data to this article can be found online at https://doi.org/10.1016/j.fuproc.2023.107881.

References

[1] L.J.R. Nunes, T.P. Causer, D. Ciolkosz, Biomass for energy: a review on supply chain management models, Renew. Sust. Energ. Rev. 120 (2020), 109658.
[2] A. Mlonka-Mędrala, A. Magdziarz, M. Gajek, K. Nowińska, W. Nowak, Alkali metals association in biomass and their impact on ash melting behaviour, Fuel 261 (2020), 116421.
[3] Y. Ge, S. Ding, X. Kong, E. Kantarelis, K. Engvall, J.B.C. Pettersson, Real-time monitoring of alkali release during co2 gasification of different types of biochar, Fuel 327 (2022), 125102.
[4] W. Weng, Q. Gao, Z. Wang, R. Whiddon, Y. He, Z. Li, M. Aldén, K. Cen, Quantitative measurement of atomic potassium in plumes over burning solid fuels using infrared-diode laser spectroscopy, Energy Fuel 31 (2017) 2831–2837.
[5] W. Weng, M. Costa, M. Aldén, Z. Li, Single particle ignition and combustion of pulverized pine wood, wheat straw, rice husk and grape pomace, Proc. Combust. Inst. 37 (2019) 2663–2671.
[6] K. Li, W. Yan, X. Huang, L. Yu, Y. Chen, C. Lou, In-situ measurement of temperature and potassium concentration during the combustion of biomass pellets based on the emission spectrum, Fuel 289 (2021), 119863.
[7] Y. Liu, Z. Wang, J. Xia, L. Vervisch, K. Wan, Y. He, R. Whiddon, H. Bahai, K. Cen, Measurement and kinetics of elemental and atomic potassium release from a burning biomass pellet, Proc. Combust. Inst. 37 (2019) 2681–2688.
[8] H. Fatehi, Z.S. Li, X.S. Bai, M. Aldén, Modeling of alkali metal release during biomass pyrolysis, Proc. Combust. Inst. 36 (2017) 2243–2251.
[9] H. Fatehi, Y. He, Z. Wang, Z.S. Li, X.S. Bai, M. Aldén, K.F. Cen, Libs measurements and numerical studies of potassium release during biomass gasification, Proc. Combust. Inst. 35 (2015) 2389–2396.
[10] Z. He, C. Lou, J. Fu, M. Lim, Experimental investigation on temporal release of potassium from biomass pellet combustion by flame emission spectroscopy, Fuel 253 (2019) 1378–1384.
[11] J. He, J. Li, Q. Huang, J. Yan, Release characteristics of potassium and sodium during pellet combustion of typical msw fractions using the Fes method, Combust. Flame 244 (2022), 112233.
[12] W. Weng, S. Li, M. Costa, Z. Li, Quantitative imaging of potassium release from single burning pulverized biomass char particles, Fuel 264 (2020), 116866.
[13] W. Weng, S. Li, M. Costa, Z. Li, Particle temperature and potassium release during combustion of single pulverized biomass char particles, Proc. Combust. Inst. 38 (2021) 3949–3958.
[14] N. Bie, J. Wang, P. Lv, Y. Zhang, Y. Bai, X. Song, W. Su, G. Yu, In-situ release characteristic of alkali metals during co-pyrolysis of coal and biomass in a visual fixed bed combined with laser-induced breakdown spectroscopy, Fuel 331 (2023), 125868.
[15] Z. Zhang, J. Liu, F. Shen, Z. Wang, Temporal release behavior of potassium during pyrolysis and gasification of sawdust particles, Renew. Energy 156 (2020) 98–106.
[16] K. Gürel, D. Magalhães, F. Kazanç, The effect of torrefaction, slow, and fast pyrolysis on the single particle combustion of agricultural biomass and lignite coal at high heating rates, Fuel 308 (2022), 122054.
[17] Y. Chen, Z. Luo, M. Fang, Q. Wang, Migration and transformation of sodium during staged coal combustion of zhundong coal and influence of carbon coating, Fuel Process. Technol. 203 (2020), 106382.
[19] Y. Xu, C. Axt, M. Song, R. Kneer, S. Li, Investigation on ignition behaviors of pulverized coal particles in a tubular swirl burner, Proc. Combust. Inst. 38 (2021) 4179–4188.
[20] X. Wen, H. Nicolai, H. Schneider, L. Cai, J. Janicka, H. Pitsch, C. Hasse, Flamelet les of a swirl-stabilized multi-stream pulverized coal burner in air and oxy-fuel atmospheres with pollutant formation, Proc. Combust. Inst. 38 (2021) 4141–4149.
[21] X. Wen, H. Nicolai, O.T. Stein, J. Janicka, A. Kronenburg, C. Hasse, Effects of air and oxy-fuel atmospheres on flamelet modeling of pollutant formation in laminar counterflow solid fuel flames, Fuel 285 (2021), 119079.
[22] J. Zhao, Y. Zhang, X. Wei, T. Li, Y. Qiao, Chemisorption and physisorption of fine particulate matters on the floating beads during zhundong coal combustion, Fuel Process. Technol. 200 (2020), 106310.
[23] T. Hirano, J. Kikkawa, F.G. Rinaldi, K. Kitawaki, D. Shimokuri, E. Tanabe, T. Ogi, Tubular flame combustion for nanoparticle production, Ind. Eng. Chem. Res. 58 (2019) 7193–7199.
[24] W. Zhu, X. Li, R. Sun, Y. Yan, M. Yuan, X. Ren, X. Meng, X. Yu, Dynamic behaviors of the sodium, calcium and iron release during coal combustion using multi-point libs, Combust. Flame 244 (2022), 112237.
[25] Y. Liu, Y. He, Z. Wang, K. Wan, J. Xia, J. Liu, K. Cen, Multi-point libs measurement and kinetics modeling of sodium release from a burning zhundong coal particle, Combust. Flame 189 (2018) 77–86.
[26] E. Thorin, K. Zhang, D. Valiev, F.M. Schmidt, Simultaneous detection of k, Koh, and kcl in flames and released from biomass using photofragmentation tdlas, Opt. Express 29 (2021) 42945.
[27] W. Weng, M. Aldén, Z. Li, Quantitative imaging of koh vapor in combustion environments using 266 nm laser-induced photofragmentation fluorescence, Combust. Flame 235 (2022) 111713.
[28] W. Weng, M. Aldén, Z. Li, Insight into Koh and Kcl Release Behavior of Burning Wood and Straw Pellets Using Quantitative In Situ Optical Measurements, Proc. Combust, Inst, 2022.
[29] Z. Qu, E. Steinvall, R. Ghorbani, F.M. Schmidt, Tunable diode laser atomic absorption spectroscopy for detection of potassium under optically thick conditions, Anal. Chem. 88 (2016) 3754–3760.
[30] E. Schlosser, T. Fernholz, H. Teichert, V. Ebert, In situ detection of potassium atoms in high-temperature coal-combustion systems using near-infrared-diode lasers, Spectroc. Acta Pt. A-Molec. Biomolec. Spectr. 58 (2002) 2347–2359.
[31] Z. Qu, P. Holmgren, N. Skoglund, D.R. Wagner, M. Broström, F.M. Schmidt, Distribution of temperature, h2o and atomic potassium during entrained flow biomass combustion – coupling in situ tdlas with modeling approaches and ash chemistry, Combust. Flame 188 (2018) 488–497.
[32] Z. Qu, F.M. Schmidt, In situ h2o and temperature detection close to burning biomass pellets using calibration-free wavelength modulation spectroscopy, Appl. Phys. B Lasers Opt. 119 (2015) 45–53.
[33] A. Sepman, Y. Ögren, Z. Qu, H. Wiinikka, F.M. Schmidt, Real-time in situ multi-parameter tdlas sensing in the reactor core of an entrained-flow biomass gasifier, Proc. Combust. Inst. 36 (2017) 4541–4548.
[34] T. Sorvajärvi, N. Demartini, J. Rossi, J. Toivonen, In situ measurement technique for simultaneous detection of k, kcl, and Koh vapors released during combustion of solid biomass fuel in a single particle reactor, Appl. Spectrosc. 68 (2014) 179–184.
[35] M.A. Bolshov, Y.A. Kuritsyn, Y.V. Romanovskii, Tunable diode laser spectroscopy as a technique for combustion diagnostics, Spectrochim. Acta B At. Spectrosc. 106 (2015) 45–66.
[36] F. Xie, R. Wu, J. Wei, X. Song, J. Li, P. Lv, J. Wang, G. Yu, Investigation on the oh*and ch* chemiluminescence characteristics of single coal particle flames under o2/co2 atmosphere, Fuel Process. Technol. 225 (2022), 107059.
[37] Y. Liu, M. Geier, A. Molina, C.R. Shaddix, Pulverized coal stream ignition delay under conventional and oxy-fuel combustion conditions, Int. J. Greenh. Gas Control 5 (2011) S36–S46.
[38] A. Molina, C.R. Shaddix, Ignition and devolatilization of pulverized bituminous coal particles during oxygen/carbon dioxide coal combustion, Proc. Combust. Inst. 31 (2007) 1905–1912.
[39] A. Carvalho, M. Rabaçal, M. Costa, M.U. Alzueta, M. Abián, Effects of potassium and calcium on the early stages of combustion of single biomass particles, Fuel 209 (2017) 787–794.
[40] L. Deng, T. Zhang, D. Che, Effect of water washing on fuel properties, pyrolysis and combustion characteristics, and ash fusibility of biomass, Fuel Process. Technol. 106 (2013) 712–720.
[41] Á.D.G. Llamas, N. Guo, T. Li, R. Gebart, K. Umeki, Rapid change of particle velocity due to volatile gas release during biomass devolatilization, Combust. Flame 238 (2022), 111898.
[42] L. Shan, M. Kong, T.D. Bennet, A.C. Sarroza, C. Eastwick, D. Sun, G. Lu, Y. Yan, H. Liu, Studies on combustion behaviours of single biomass particles using a visualization method, Biomass Bioenergy 109 (2018) 54–60.
[46] P.J. van Eyk, P.J. Ashman, Z.T. Alwahabi, G.J. Nathan, The release of water-bound and organic sodium from loy yang coal during the combustion of single particles in a flat flame, Combust. Flame 158 (2011) 1181–1192.
[47] P.J. van Eyk, P.J. Ashman, Z.T. Alwahabi, G.J. Nathan, Quantitative measurement of atomic sodium in the plume of a single burning coal particle, Combust. Flame 155 (2008) 529–537.
[48] S. Lith, P.A. Jensen, F.J. Frandsen, P. Glarborg, Release to the gas phase of inorganic elements during wood combustion. Part 2: influence of fuel composition, Energy Fuels 22 (2008).
[49] M.J. Wornat, R.H. Hurt, N.Y.C. Yang, T.J. Headley, Structural and compositional transformations of biomass chars during combustion, in: United States, 1995, pp. 131–143. https://go.exlibris.link/sZWW9HzY.
[50] C.Z. Li, C. Sathe, J.R. Kershaw, Y. Pang, Fates and roles of alkali and alkaline earth metals during the pyrolysis of a victorian brown coal, Fuel 79 (2000) 427–438.
[51] T. Khazraie Shoulaifar, N. Demartini, M. Zevenhoven, F. Verhoeff, J. Kiel, M. Hupa, Ash-forming matter in torrefied birch wood: changes in chemical association, Energy Fuel 27 (2013) 5684–5690.
[52] J. Zhang, C.L. Han, Z. Yan, The varying characterization of alkali metals (na, k) from coal during the initial stage of coal combustion, Energy Fuel 15 (2001) 786–793.
[53] E. Björkman, B. Strömberg, Release of chlorine from biomass at pyrolysis and gasification conditions1, Energy Fuel 11 (1997) 1026–1032.
[54] Y. Liu, L. Cheng, Y. Zhao, J. Ji, Q. Wang, Z. Luo, Y. Bai, Transformation behavior of alkali metals in high-alkali coals, Fuel Process. Technol. 169 (2018) 288–294.
[55] M.U. Rahim, X. Gao, M. Garcia-Perez, Y. Li, H. Wu, Release of chlorine during mallee bark pyrolysis, Energy Fuel 27 (2013) 310–317.
[56] A. Kosminski, D.P. Ross, J.B. Agnew, Transformations of sodium during gasification of low-rank coal, Fuel Process. Technol. 87 (2006) 943–952.
[57] Y. Liu, Z. Wang, K. Wan, Y. Lv, J. Xia, Y. He, K. Cen, In situ measurements of the release characteristics and catalytic effects of different chemical forms of sodium during combustion of zhundong coal, Energy Fuel 32 (2018) 6595–6602.
[59] A. Joppich, H. Salman, Wood powder feeding, difficulties and solutions, Biomass and Bioenergy 16 (1999) 191–198.
[60] J. Dai, H. Cui, J.R. Grace, Biomass feeding for thermochemical reactors, Prog. Energy Combust. Sci. 38 (2012) 716–736.